HHS Public Access

Author manuscript

Mucosal Immunol. Author manuscript; available in PMC 2018 June 20.

Published in final edited form as:

Mucosal Immunol. 2018 May ; 11(3): 932–946. doi:10.1038/mi.2017.112.

Early Treatment of SIV+ macaques with an $\alpha_4\beta_7$ mAb alters virus distribution and preserves CD4+ T cells in later stages of infection

Philip J. Santangelo[1,*,#], **Claudia Cicala**[2,#], **Siddappa N. Byrareddy**[4,#], **Kristina Ortiz**[2], **Dawn Little**[2], **Kevin E. Lindsay**[1], **Sanjeev Gumber**[5], **J. J. Hong**[5], **Katija Jelicic**[2], **Kenneth A. Rogers**[6], **Chiara Zurla**[1], **Francois Villinger**[6], **Aftab A. Ansari**[3], **Anthony S. Fauci**[2], and **James Arthos**[2,*]

[1]Walter H. Coulter Department of Biomedical Engineering, Georgia Institute of Technology and Emory University, 313, Ferst Drive Atlanta, GA 30680

[2]Laboratory of Immunoregulation, National Institutes of Allergy & Infectious Diseases, National Institutes of Health, Bethesda, MD 20814

[3]Department of Pathology, Emory University School of Medicine, Atlanta, GA 30322

[4]Department of Pharmacology and Experimental Neuroscience, University of Nebraska Medical Center, Omaha, NE 68198

[5]Division of Microbiology & Immunology, The Yerkes National Primate Research Center, Emory University, Atlanta, GA 30322

[6]New Iberia Research Center, University of Louisiana Lafayette, Lafayette, LA, 70560

Abstract

Integrin $\alpha_4\beta_7$ mediates the trafficking of leukocytes, including $CD4^+$ T cells, to lymphoid tissues in the gut. Virus mediated damage to the gut is implicated in HIV and SIV mediated chronic immune activation and leads to irreversible damage to the immune system. We employed an immuno-PET/CT imaging technique to evaluate the impact of an anti-integrin $\alpha_4\beta_7$ mAb alone or in combination with ART, on the distribution of both SIV infected cells and $CD4^+$ cells in rhesus macaques infected with SIV. We determined that $\alpha_4\beta_7$ mAb reduced viral antigen in an array of tissues of the lung, spleen, axillary and inguinal lymph-nodes. These sites are not directly linked to

*To whom correspondence should be addressed: Dr. Philip J. Santangelo Georgia Institute of Technology, 225 North Ave NW, Atlanta, GA, 30332; philip.santangelo@bme.gatech.edu and Dr. James Arthos, Laboratory of Immunoregulation, Bldg. 10, Room 6A08, NIH, 9000 Rockville, MD 20892; jarthos@niaid.nih.gov.
#These authors contributed equally.

Author contributions: The nonhuman primate studies were designed and overseen by JA, CC, FV and AAA. The laboratory-based studies were conducted by SNB, JJH, KER, and SG with technical assistance by KO and DL. The PET/CT imaging studies were designed and planned by PJS, FV, JA, SNB and AAA. PET probes were produced by CZ, and PET analysis by PJS. Statistical analysis was performed by SG, KL and PS. JA, PJS, KJ and AAA prepared the draft of this manuscript with input from all the authors. A.S.F. provided discussions and review of the manuscript.

DISCLOSURE

The authors declared no conflict of interest.

$\alpha_4\beta_7$ mediated homing, however the most pronounced reduction in viral load was observed in the colon. Despite this reduction, $\alpha_4\beta_7$ mAb treatment did not prevent an apparent depletion of the $CD4^+$ cell in gut in the acute phase of infection that is characteristic of HIV/SIV infection. However, $\alpha_4\beta_7$ mAb appeared to facilitate the preservation or restoration of $CD4^+$ T cells in gut tissues at later stages of infection. Since damage to the gut is believed to play a central role in HIV pathogenesis, these results support further evaluation of $\alpha_4\beta_7$ antagonists in the study and treatment of HIV disease.

Introduction

During the acute phase of HIV and SIV infection, $CD4^+$ T cells are massively depleted in gut associated lymphoid tissue (GALT) [1, 2, 3, 4]. Coincident with $CD4^+$ T cell depletion, the gut architecture is disrupted in a manner that prevents the proper re-seeding of gastro-intestinal tissues (GALT) with lymphoid cells, including $CD4^+$ T cells[5]. The damage to the gut ultrastructure is largely irreversible, even after effective long-term intervention with highly active anti-retroviral drug therapies (ART), [6, 7, 8, 9, 10]. The mechanisms that underlie this irreversible pathology are not fully defined. One view is that mucosal tissues gradually become fibrotic in response to chronic viral infection and consequently immune responses are impaired. This view is supported by the successful use of anti-fibrotic therapy, which promotes a partial reconstitution of $CD4^+$ T cells in the gut [11]. It has been further suggested that the disruption of the gut architecture promotes leakage of gut bacteria to the systemic circulation, and that this bacterial translocation leads to chronic immune activation [12]. As such, GALT dysfunction contributes to the increased and accelerated incidence of co-morbidities and a lifetime of disability. Such pathologies appear and persist despite ART-based chemotherapy of HIV-1 infected individuals [13, 14, 15].

In efforts to develop interventions that minimize GALT pathology secondary to HIV/SIV infection, we have carried out a series of studies focused on lymphocytes that migrate into GALT and subsequently mediate inflammatory responses. Prominent among activated cells trafficking to GALT are those that express $\alpha_4\beta_7$ integrin ($\alpha_4\beta_7$), the gut homing receptor [16]. $\alpha_4\beta_7^+/CD4^+$ T cells are preferred targets for HIV/SIV infection in vitro and in vivo [17, 18, 19, 20, 21]. We reasoned that by targeting $\alpha_4\beta_7$ would interfere with the trafficking and/or infection of a key subset of $CD4^+$ T cells that HIV and SIV infect in the early stages of infection. Antibodies and antagonists specific to $\alpha_4\beta_7^+$ are being actively developed for the treatment of inflammatory bowel disease [22].

In order to target $\alpha_4\beta_7^+/CD4^+$ T cells we derived a “primatized” recombinant monoclonal mAb with specificity for the heterodimeric form of $\alpha_4\beta_7$. This recombinant antibody ($\alpha_4\beta_7$ mAb) was found to have limited immunogenicity in rhesus macaques, allowing for repeated administration in vivo [23]. In a series of studies we demonstrated that $\alpha_4\beta_7$ mAb exerts a profound impact on both viral replication in GALT, and disease progression. Administration just prior to and during acute infection led to marked reductions in viral loads in the GALT of rhesus macaques infected intravenously [24] or intra-rectally [25]. In the intravenous challenge study, $\alpha_4\beta_7$ mAb-treated animals remain healthy five years post infection while IgG treated control animals all died within two years. In a third study, administration of

$\alpha_4\beta_7$ mAb just prior to and during repeated low dose vaginal exposures to SIV mac251 reduced, in a significant way, the efficiency of transmission [20]. Of note, in each of these studies, while the viral loads in the GALT of $\alpha_4\beta_7$ mAb treated animals were reduced compared to control animals, the plasma viral loads of control and $\alpha_4\beta_7$ mAb treated animals were similar. Further evidence of the key role for $\alpha_4\beta_7^+$/CD4$^+$ T cells comes from a recent study in which we treated macaques five weeks post-SIV infection with either a 90 day course of ART, or a combination of ART and $\alpha_4\beta_7$ mAb. Macaques that received ART + IgG showed high viral load rebounds once ART was removed. These animals succumbed to AIDS within two years. In contrast, those receiving the combination therapy were able to control plasma viremia to very low or undetectable levels, and low or undetectable levels of pro-viral DNA were maintained in GALT. More than three years later these animals remain healthy [26]. Taken together these studies suggest that a dynamic interplay between $\alpha_4\beta_7^+$/CD4$^+$ T cells and GALT may be central to HIV/SIV disease. $\alpha_4\beta_7$ mAb has the potential to disrupt this interplay in several ways. It interferes with $\alpha_4\beta_7$ binding to its natural ligands (MAdCAM and VCAM), but also to SIV gp120[27]. Understanding how $\alpha_4\beta_7$ mAb alters the distribution of SIV is an important first step in defining the mechanism by which $\alpha_4\beta_7$ mAb alters the interplay between SIV and $\alpha_4\beta_7^+$/CD4$^+$ T cells, and may provide key insights into the nature of HIV/AIDS disease.

As noted above, viral replication in, and destruction of GALT is a defining feature of acute HIV and SIV infection. HIV and SIV mediated destruction of gut ultrastructure is likely irreversible. In previously published studies we determined that treatment with $\alpha_4\beta_7$ mAb can alter SIV-mediated pathogenesis in a significant way[20, 23, 24]. We reasoned that understanding how and where $\alpha_4\beta_7$ mAb impacts viral replication may provide important insights into HIV pathogenesis. Because $\alpha_4\beta_7$ is the only integrin capable of binding to MAdCAM, the tissue-specific expression of MAdCAM defines $\alpha_4\beta_7$ as the gut homing integrin. MadCAM is expressed throughout the gut. It is expressed at high levels on endothelial cells lining the lumen of high endothelial venules (HEV) in the intestinal lamina propria, Peyer's patches and mesenteric lymph nodes, as well as on follicular dendritic cells (DC) in the gut mucosa.

To this end we utilized conventional immunological and virological techniques in conjunction with a newly developed non-invasive PET/CT imaging technique to determine where in the gut and throughout the body $\alpha_4\beta_7$ mAb changes viral replication. PET/CT was utilized as it is a whole-body, highly sensitive molecular imaging methodology compatible with macaques, with spatial resolution sufficient to interrogate changes within the gut. Our imaging technique involves the intravenous administration of a ^{64}Cu/DOTA labeled, polyethylene glycol-conjugated anti-SIV gp120 mAb (clone 7D3) that provides footprints and localization of infected cells in vivo [28]. To complement this approach, we developed a related imaging protocol, described herein, which utilizes a CD4 receptor specific ^{64}Cu/DOTA labeled anti-CD4 antibody fragment (F(ab′)$_2$). This probe allows us to obtain images of CD4$^+$ cells in live animals.

With these probes we sought to identify differences in the localization of SIV infected cells in rhesus macaques administered with the $\alpha_4\beta_7$ mAb alone or in combination with ART, compared to control animals. We also examined differences in the in vivo distribution of

$CD4^+$ cells during the acute and the chronic phases of infection. In conjunction with our image analysis, we obtained a large number of different tissues biopsies from live animals and also at autopsy and quantitated the levels of SIV pro-viral DNA and $CD4^+$ T cells. As we report below, our image analysis allowed us to better understand how $\alpha_4\beta_7$ mAb treatment protects GALT from SIV mediated damage in a way that alters the course of disease.

Results

Imaging Cohorts

PET/CT imaging studies were carried out on representative animals from three separate treatment cohorts of SIV infected macaques that were treated with $\alpha_4\beta_7$ mAb (Supplementary Figure 1 and Supplementary Table 1). One set of images was obtained from animals 2–3 weeks post-infection and this cohort is referred to as the acute cohort. Another set of images was obtained from animals 16–17 weeks post-infection, and this cohort is referred to as the early-chronic cohort (Supplementary Figure 1). A third set of images was obtained from animals treated with a combination of ART, beginning five weeks post infection, and $\alpha_4\beta_7$ mAb, beginning nine weeks post infection (Supplementary Figure 1). This cohort is referred to as the dual-therapy cohort. Animals from the early-chronic cohort and dual therapy cohorts were described in detail elsewhere [20, 26]. Animals in the acute cohort were infected and treated in an identical manner to animals described in detail in two published studies using either high-dose intra-rectal (IR) or high-dose intravenous (IV) challenge [24, 25]. In brief, the macaques in the acute infection cohort received either 50 mg/kg of a “primatized” recombinant $\alpha_4\beta_7$ monoclonal antibody or 50 mg/kg of normal recombinant rhesus IgG intravenously on day −3 and again on day 21. On day 0 animals were infected either IR with 500 $TCID_{50}$ of SIVmac251 or IV with 200 $TCID_{50}$ of SIVmac239. Macaques in the early-chronic infection cohort received the primatized $\alpha_4\beta_7$ mAb or recombinant rhesus IgG IV on day −3 and the same dose every 3 weeks for 12 weeks. On day 0 and each week thereafter these animals were challenged with a low-dose of SIV mac251 intra-vaginally until week 5, at which point ten out of the twelve IgG-treated animals had become infected. In contrast, treatment with $\alpha_4\beta_7$ mAb prevented transmission in 6/12 animals. The remaining 6 animals in this group did, with some delay, become infected and they are among the animals employed in this imaging study. Animals in the dual-therapy cohort were treated with a 90-day course of ART initiated at 5 weeks post infection followed at 9 weeks post infection by 8 infusions of $\alpha_4\beta_7$ mAb administered every 3 weeks until week 32. Subsequently all animals treated with this regimen maintained low or undetectable plasma viremia for at least three years.

Plasma and Tissue Viral Loads in acute and early-chronic cohorts

To complement the imaging studies described below, we determined both plasma and tissue levels of SIV by PCR from animals in both the acute and early-chronic cohorts. We first compared viral loads in the plasma of $\alpha_4\beta_7$ mAb vs. IgG-treated animals from both cohorts and determined that, collectively, the $\alpha_4\beta_7$ mAb treated animals showed a non-significant reduction (~0.5–1.0 log) in peak plasma viral loads relative to animals treated with IgG (Figure 1a). This observation is in good agreement with our previous determinations that

$\alpha_4\beta_7$ mAb treatment alone does not reduce SIV plasma viral loads in a significant way [20, 24]. We next addressed the impact of $\alpha_4\beta_7$ mAb treatment on viral replication in specific tissues and/or organs. Pro-viral DNA levels were obtained by PCR from an extensive panel of tissues biopsies and organs taken at necropsy from both cohorts. Necropsies were conducted within one week following the PET/CT imaging that is described below. Because the data on levels of viral DNA in specific tissues from the two treatment groups in both cohorts were similar, data from the two cohorts were pooled and presented together (Fig 1b, c, d). This allowed for an increase in sample size per tissue analyzed. When comparing pro-viral DNA levels in tissues from the two treatment groups we observed a statistically significant decrease ($p < 0.001$) in pro-viral DNA loads in the jejunum, ileum and colon of the macaques that received $\alpha_4\beta_7$ mAb as compared to those that received IgG (Figure 1b). Regarding the viral loads found in various lymph-nodes, we found that the IgG-treated animals carried higher amounts of pro-viral DNA in mesenteric, axillary (> 1000 copies/ng DNA) and inguinal lymph-nodes (> 100 copies/ng DNA) than in $\alpha_4\beta_7$ mAb-treated animals (~10 copies/ng DNA) (Figure 1d).

Little difference was observed in the colonic and internal iliac lymph-nodes from the two groups of animals (Figure 1d). Assessment of other organs and tissues showed that pro-viral DNA loads trended lower in the $\alpha_4\beta_7$-mAb group, most notably in lung, tonsils and spleen, but also in bone marrow (Figure 1c). For lungs, tonsils and the splenic tissues these differences were > 1 log. In contrast, similar viral DNA levels were found in liver tissues from both treatment groups (Figure 1c). In summary, these data suggest that, in general, cells residing within GALT had lower pro-viral DNA loads in the $\alpha_4\beta_7$-treated animals as compared to control IgG-treated animals. Surprisingly, pro-viral loads in several peripheral lymph-nodes and organs not normally associated with $\alpha_4\beta_7$-mediated homing were also reduced in $\alpha_4\beta_7$ mAb-treated animals.

Immuno-PET/CT based image analysis

The tissue-specific impact of $\alpha_4\beta_7$ mAb treatment on viral loads described above complimented our efforts to investigate the distribution of virus in these animals using a novel immuno-PET/CT imaging technique. This technique involves the infusion of a ^{64}Cu-labeled probe just prior to PET/CT imaging [28]. To image virus infected cells we employed an SIV env specific non-neutralizing probe based on the mAb 7D3[28]. Several examples of this technique are provided (Supplementary Figures 2 and 3), in which we have identified organs of interest for SIV interrogation, in both PET and CT images (Supplementary Figure 2), and compared anti-gp120 signals obtained in a macaque chronically infected with SIVmac251 as well as an uninfected macaque (Supplementary Figure 3). In Supplementary Figure 3 both macaques received the same dose of ^{64}Cu-labeled mAb 7D3, however marked differences are evident, with the infected macaque exhibiting substantially higher signals.

Immuno-PET/CT image analysis of SIV gp120 during acute infection

To assess the impact of $\alpha_4\beta_7$ mAb on the localization of virus in live animals during the acute phase of infection we acquired anti-gp120 immuno-PET/CT images from two macaques pretreated with $\alpha_4\beta_7$ mAb (RQl15, RPj15) and two animals pretreated with control IgG (RSq14, RPg15). Images were acquired at both 2 and 3 weeks post-infection.

Images from representative animals at 3 weeks PI are presented in Figure 2, while imaging quantification results from 2 weeks PI are presented in Supplementary Figure 4. SUVmax values are listed in Supplementary Tables 2 and 3. Representative images of the GI tract from two animals at three weeks PI are presented in Figure 2a, and average SUVmax values (the maximal signal obtained within the tissue/organ) from various tissues measured in all four animals three weeks PI are provided (Figure 2b and Supplementary Table 2). When the SUVmax values from the spleen, inguinal LN, axillary LN, lung, colon, small bowel and genital tract from all four animals were measured we generally observed reduced signals in the $\alpha_4\beta_7$ mAb-treated animals vs. the IgG-treated controls. A similar, although less pronounced result was observed at week 2 (Supplementary Figure 4). Using a hierarchical ANOVA differences in the signals were determined to be significant ($p = 0.0382$). Signals derived from cross-sections (CS) of the small bowel and colon 3 weeks PI yielded similar results, mainly a lower signal in $\alpha_4\beta_7$ mAb-treated animals vs. the IgG-treated controls (Figure 2c). Average SUVmax values from CS images of all four animals are presented in Figure 2d and supplementary Table 3. gp120 signals were lower in $\alpha_4\beta_7$ mAb treated animals in both the upper and lower CS ($p = 0.0003$ and $p = 0.0002$ respectively) (Figure 2c and d and Supplementary Table 3). Thus, our image analysis revealed that the administration of the $\alpha_4\beta_7$ mAb mediated a reduction of virus in both GALT and other immune tissues at these early time points. These reductions were found in animals infected either intra-rectally or intravenously (Supplementary Table 1), and are consistent with the PCR results described above (Figure 1).

Immuno-PET/CT image analysis of SIV during early-chronic infection

We next asked how repeated administration of $\alpha_4\beta_7$ mAb through the early-chronic phase of infection impacted viral replication in various tissues, including GALT. Similar immuno-PET/CT-based imaging as described above was performed on two pairs of infected macaques that received either $\alpha_4\beta_7$ mAb or control IgG every three weeks from day 3 prior to infection up to week 12 (5 infusions, 50mg/kg). Images were acquired at weeks 16–17 (Fig 3). These two pairs of macaques were chosen based upon similar plasma viral loads. In this manner RLc12 (IgG-treated) was paired with RDg11 ($\alpha_4\beta_7$ mAb-treated) and RRn11 (IgG-treated) was paired with RCw11 ($\alpha_4\beta_7$ mAb-treated). The first pair (RLc12/RDg11) exhibited relatively high viral loads when compared to the second pair (RRn11/RCw11). Representative images of GALT obtained from each of these four macaques are included, (Figure 3a) with the small bowel and colon highlighted. Although RDg11($\alpha_4\beta_7$ mAb treated) exhibited a nominally higher plasma viral load than RLc12 (IgG treated) (7,926,573 vs. 3,403,352) average SUVmax values in GALT, nasal -associated lymphoid tissue (NALT), spleen, inguinal LN, and lungs were lower (Figure 3b upper panel and Supplementary Table 4). Similarly RRn11 and RCw11 presented low plasma viral loads of 401,692 and 257, 966 respectively, around the time of imaging, Supplementary Table 4). SUVmax values in GALT, lung, and spleen were markedly lower in RCw11 ($\alpha_4\beta_7$ mAb treated) (Figure 3b and Table S4). Lower signals in $\alpha_4\beta_7$ mAb treated animals were also apparent in both pairs of animals when comparing CS images (Figure 3c). An interesting point becomes evident when the SUVmean values for the colon and small bowel were compared. Treatment does not appear to alter the signals acquired from the small bowel (Figure 3b middle-lower panel, and Table S5. However, $\alpha_4\beta_7$ mAb treatment was associated with lower signals in the colon.

This differential effect is illustrated in Figure 3b bottom panel which presents the ratio of the SUVmeans of the colon/small bowel for each animal. This effect is likely related to the well-established role for $\alpha_4\beta_7$ as the major mediator of lymphocyte trafficking to the colon, whereas other trafficking receptors such as CCR9, in addition to $\alpha_4\beta_7$ can facilitate trafficking to the small bowel [29, 30]. These data demonstrate that $\alpha_4\beta_7$-mAb treatment in SIV infected rhesus macaques changes the viral distribution within different tissues of the gut, which is noteworthy considering its impact on disease progression.

Immuno-PET/CT in vivo image analysis of CD4$^+$ cells

We employed a ^{64}Cu-labeled anti-CD4 F(ab′)$_2$ derived from a non-depleting CD4 mAb as a probe, to develop a method to image CD4$^+$ cells. In the course of optimizing this probe we explored the inter-animal CD4 signal variability in various tissues from four uninfected macaques. Images from 3 of these animals are displayed in Figure 4 (RBv10) and in Supplementary Figure 5a (RVg13, and RWg13), and quantitative data from these three animals and a fourth animal (RVE7) shown in Supplementary Figure 5b. All four animals revealed CD4$^+$ signals in the colon, small bowel, genital tract, spleen, NALT, axillary, inguinal and facial cranial LNs. Negligible signals were observed in muscle tissue. Although there was some inter-animal variation in SUVmax values, the relative values in each tissue were generally consistent. The most prominent signals appeared in the spleens of all four animals. We calculated the ratio of SUVmax for these two tissues in each of the four animals (Supplementary Figure 5b), and found that increases in SUVmax between spleen and the GI tract ranged from 3–8 fold (Supplementary Figure 5c). To assess the overall specificity and sensitivity of our CD4 PET imaging technique we injected two healthy uninfected macaques with a dual labelled ^{64}Cu and Dylight 650 anti-CD4 F(ab′)$_2$ imaging probe. PET/CT images were acquired and animals were subsequently sacrificed and necropsied. Isolated CD3+ positive cells from various tissues and organs were then analyzed by flow-cytometry with a second, noncompeting anti CD4 fluorescent mAb (Supplementary Figure 6a). The percent of CD3+CD4+ cells detected by the in vivo and in vitro derived fluorescent signals were found to be within 5% in all tissues/organs measured, demonstrating that the in vivo delivered probe detects CD4+ T cells in a specific manner (Supplementary Figure 6b). The sensitivity of the CD4 imaging was determined using the spleen as a model organ (Supplementary Figure 6c). Using flow cytometry, the number of probe-positive cells per gram of tissue was calculated. The mass of the spleen was approximated at 7 grams, allowing for an approximation of the total number of probe-positive cells per spleen. The ratio of total probe-positive cells to total SUV was calculated (Supplementary Figure 6c and methods). This ratio was then used to calculate the sensitivity based on a minimum signal of 2, which was approximately 3400 cells.

We next compared the signals obtained following anti-CD4 mAb administration in SIV infected vs. uninfected macaques. Representative PET/CT imaging results from four animals are shown in Figure 4. An uninfected animal (RBv10), (Fig 4A far left panels), along with a chronically infected animal who presented an absolute CD4 count of < 200 around the time of imaging (RZB9), and an uninfected animal treated with the IgG control probe (RVe7). Strong CD4$^+$ signals were apparent, as expected, in all of the lymphoid organs of RBv10 (uninfected) including the axillary LNs, inguinal LNs, spleen and throughout the GI tract. In

contrast, signals were sharply reduced in the axillary lymph-nodes, facial cranial lymph-nodes, GI tract, the inguinal/popliteal lymph-nodes, and the spleen of RZB9 (chronically infected) (Figure 4a middle left panels). Differences in the intensity of SUVmax values for the axillary and inguinal lymph-nodes, the colon, small bowel and spleen in four uninfected, and two chronically infected animals probed with anti CD4 and two animals that were probed with control IgG (Supplementary Table 1) are presented in Figure 4b. Using an ANOVA on the SUV max values across all organs we determined that CD4 signals were significantly lower in the chronically infected animals ($p < 4.7\times10^{-5}$), which is consistent with the depletion of $CD4^+$ T cells secondary to viral infection. It is also possible that the reduction of signal occurred as a consequence of CD4 receptor downregulation secondary to infection, an event that typically precedes cell death. The relative decreases in signal between infected and uninfected macaques was most apparent in the colon, consistent with previous findings of profound SIV-mediated depletion of $CD4^+$ T cells within this organ [31]. Of note, in RZB9 (Figure 4a) we observed pockets of low signal in sections of the axillary and facial cranial LN, suggesting that residual $CD4^+$ cells remain in these tissues in the face of chronic infection. A comparison of the images obtained from RVe7, an infected animal that was administered a ^{64}Cu-labeled rhesus $F(ab')_2$ derived from normal IgG, confirms that the small pockets of low signal in RZB9 likely represent specific binding of the ^{64}Cu-labeled CD4 mAb to $CD4^+$ cells.

Overall these data lead us to conclude that our method of identifying $CD4^+$ cells is sufficiently specific and sensitive for the detection of $CD4^+$ cells in the major lymphoid tissues throughout the body, including GALT. Importantly, with this method, enabled us to detect the depletion and/or redistribution of $CD4^+$ cells in the tissues of a chronically infected macaque.

Immuno-PET/CT image analysis of $CD4^+$ cells during acute infection in animals treated with an $\alpha_4\beta_7$ mAb

We next asked how $\alpha_4\beta_7$ mAb treatment impacts the localization of $CD4^+$ cells during acute SIV infection. Images were acquired from 4 rhesus macaques (Supplementary Table 1). Two received $\alpha_4\beta_7$ mAb intravenously on day −3 prior to infection, and a second infusion 3 weeks PI. The second pair of macaques received rhesus IgG. Two and five weeks post-infection animals were administered the ^{64}Cu-labeled anti-CD4 $F(ab')_2$ and imaged by PET/CT. Representative images from axillary lymph-nodes, facial cranial lymph-nodes, GI tract, the inguinal/popliteal lymph-nodes, and the spleen of an $\alpha_4\beta_7$ mAb-treated animal (ROe15) are presented in Fig 4a (far right panels). Average SUVmax values for the colon and small bowel of ROe15 and a second $\alpha_4\beta_7$ mAb treated animal (ROr14) are reported in Fig 4c, along with values from two acutely infected animals (RUp14, RVo14) treated with control IgG (Supplementary Table 1). Interestingly, $\alpha_4\beta_7$ mAb treatment had little detectable impact on the anti-CD4 SUV max values obtained for the GALT, despite decreased pro-viral DNA in GALT (Figure 1). That is, during an acute infection we could not detect any $\alpha_4\beta_7$ mAb-mediated protection of total $CD4^+$ cells in GALT relative to IgG-treated controls (no statistical differences during the acute infection, $p>0.05$). This also held true for other tissues at 5 weeks PI (Figure 4c; $p>0.05$). We then validated this observation by utilizing flow-cytometry to determine $CD4^+$ T cell frequencies from colon biopsies of six acutely infected

animals treated with either $\alpha_4\beta_7$ mAb or control IgG (Figure 5). In both $\alpha_4\beta_7$ mAb- and control IgG-treated groups we observed a ~50% reduction in the frequency of $CD4^+$ T cells in colon biopsies relative to pre-infection baseline values. Thus, $\alpha_4\beta_7$ mAb treatment did not prevent the initial reduction of $CD4^+$ cells in gut tissues that is characteristic of acute SIV infection despite its capacity to reduce pro-viral DNA in GALT (Figure 1).

$CD4^+$ T cell frequencies during early-chronic infection of SIV infected macaques treated with $\alpha_4\beta_7$ mAb

We next asked whether $\alpha_4\beta_7$ mAb treatment would impact the integrity of the $CD4^+$ T cell compartment at later stages of infection by determining the frequencies of $CD4^+$ T cells in colon biopsies of both $\alpha_4\beta_7$ mAb and IgG-treated animals during early-chronic infection. We also measured $CD4^+$ T cells later in chronic infection (after week 45), long after $\alpha_4\beta_7$ mAb was cleared from the blood of treated animals. As expected, $CD4^+$ T cell frequencies in IgG-treated animals were already >90% depleted by weeks 12–15, and these frequencies remained low into the chronic phase of infection (Figure 5). The frequencies of $CD4^+$ cells in the $\alpha_4\beta_7$ mAb-treated animals were different. Frequencies continued to decline from the levels measured during the acute phase, but not to the same degree as was observed in IgG-treated animals. The average levels in $\alpha_4\beta_7$ mAb-treated animals dropped from ~25% to ~17%, which, although reduced, remained significantly greater than the frequencies found in the IgG control animals (<3%, $p< 0.01$), suggesting that $\alpha_4\beta_7$ mAb treatment slowed the decline of $CD4^+$ cells in the colon following acute infection. From week 17 out past week 45 frequencies of $CD4^+$ cells were maintained. This is notable as the half-life of the $\alpha_4\beta_7$ mAb is ~ 11.4 days. Thus, treatment with $\alpha_4\beta_7$ mAb prior to, and during the acute phase of infection, which does not significantly reduce plasma viremia, appeared to preserve a fraction of the $CD4^+$ T cell compartment in the gut long after the therapy had ceased. This capacity to preserve $CD4^+$ T cells following the initial depletion that occurs during acute infection may reflect a generalized protection of GALT integrity.

$CD4^+$ cell imaging prior to and during $\alpha_4\beta_7$ mAb treatment in uninfected animals

Given the role of $\alpha_4\beta_7$ as a gut homing receptor [32] one might reason that the reduction of pro-viral DNA in $\alpha_4\beta_7$ mAb treated animals noted above (Figure 1) is secondary to a reduction of GALT $CD4^+$ cells, independent of SIV infection. This is the basis upon which an analogue of this mAb is being employed in the treatment of IBD [33, 34, 35]. To understand if reduced pro-viral DNA was associated with a loss of target CD4 cells in GALT we imaged 4 uninfected animals prior to treatment in order to establish their baseline $CD4^+$ PET signals (Supplementary Table 1). We then treated these animals with the $\alpha_4\beta_7$ mAb and imaged them again two weeks later with our anti-CD4 PET probe. No differences in CD4 signals were detected at either week 2 ($p= 0.935$) or at week 5 ($p = 0.856$) relative to baseline (Figure 6), indicating that a single administration of $\alpha_4\beta_7$ mAb does not lead to a gross reduction of total CD4 signals in GALT, although it likely impedes the migration of a subset of $\alpha_4\beta_7^{Hi}$ $CD4^+$ T cells. However, it is possible that alternative homing mechanisms facilitated the replacement of $\alpha_4\beta_7^{Hi}$ $CD4^+$ T cells in GALT with other $CD4^+$ T cell subsets. In addition, these animals were not experiencing any overt gut inflammation at the time of $\alpha_4\beta_7$ mAb treatment, and it is possible that in the context of an inflammatory response we might have observed a reduction in the CD4 signal.

Immuno-PET/CT image analysis of SIV and CD4 of macaques treated with ART and $\alpha_4\beta_7$ mAb

We recently reported that SIV infected macaques treated with a combination of ART and $\alpha_4\beta_7$ mAb were able to achieve sustained virologic control for > 2 years after all therapy was withdrawn (Supplementary Figure 1) [26]. The mechanism of control remains to be determined. During the dual therapy period (weeks 9–18) all animals in both treatment groups were aviremic. However, by week 15 the two treatment groups began to differ with respect to several lymphocyte subsets and plasma biomarkers, suggesting that the mechanism of off-therapy control in animals receiving $\alpha_4\beta_7$ mAb originated during this period. We have since analyzed PET/CT images of SIV gp120 in both treatment groups at week 16.

Images from two ART + $\alpha_4\beta_7$ mAb treated animals (ROq14, Rlv14) and two ART + control IgG animals (Rlo14, RUs14) at week 16, (the 9th week after plasma viremia fell below the level of detection) revealed gp120 signals in small-bowel, large intestine, spleen axillary and inguinal LNs, lungs and NALT of all four animals (Figure 7a, b). These signals are consistent with our previously published PET/CT imaging analysis of SIV infected and ART-treated macaques[28]. Of particular interest were the relatively lower overall signals in ART + $\alpha_4\beta_7$ mAb animals ($p = 0.0283$). Differences were apparent in small-bowel, spleen and large intestine, but not in lung, NALT, and inguinal and axillary LNs. Signals in the large intestine of animals treated with ART + $\alpha_4\beta_7$ mAb were ~3-fold lower when compared to ART treated animals. That such differences existed after 11 weeks of ART is difficult to explain considering it is occurring in the absence of ongoing viral replication or expression of gp120.

Additional images were acquired at week 22, 4 weeks after ART was interrupted (around the time that rebounding plasma viremia peaked in animals that received ART + control IgG) (Figure 7b). Signals increase in both treatment groups in small-bowel, large intestine, spleen, axillary LNs and lung, but remained relatively lower in the ART + $\alpha_4\beta_7$ mAb treated animals ($p=0.02135$). In both the $\alpha_4\beta_7$ treated case (p value of 0.025) and IgG case (p value of 0.0224), the SUVmax levels increased after ART interruption, but they increased less in the $\alpha_4\beta_7$ treatment group. Overall, the most striking difference between the two treatment groups was the apparent reduction in viral envelope signal in the large intestine both before and after ART interruption in the ART + $\alpha_4\beta_7$ mAb treated animals.

We also imaged $CD4^+$ cells at week 23, five weeks after ART interruption. In all tissues analyzed we detected higher $CD4^+$ signals in the ART + $\alpha_4\beta_7$ mAb treatment group relative to the ART-alone animals (Figure 8; $p=0.012$). This is consistent with decreased virus in the small intestine, large intestine, spleen, axillary LNs and lung of animals treated with + $\alpha_4\beta_7$ mAb described above (Figure 7). Finally, we also observed increased CD4 signals in inguinal LNs (Figure 8b) despite the nearly identical virus signals in inguinal LNs of both treatment groups at week 22 (Figure 7).

Discussion

We previously reported that treatment with $\alpha_4\beta_7$ mAb can have a profound impact on both transmission and pathogenesis in an SIV/Macaque model of HIV disease [20, 24], and in combination with ART, promote durable virologic control[26]. Yet the specific mechanism(s) by which this antibody achieves these effects is unknown. A unifying theme in each of those studies was the capacity of $\alpha_4\beta_7$ mAb treatment to reduce levels of pro-viral DNA in colon biopsies. Additionally, $\alpha_4\beta_7$ mAb appeared to either protect $CD4^+$ T cells in GALT, or promote their reconstitution. In this report, by imaging live animals undergoing $\alpha_4\beta_7$ mAb treatment at acute and early-chronic stages of infection we are able to show that $\alpha_4\beta_7$ mAb promoted a redistribution of viral antigen (gp120) within GALT. Moreover, $CD4^+$ cells in GALT, but also in tissues that are not associated with $\alpha_4\beta_7$ mediated trafficking were preserved. These findings suggest that protection of specific lymphoid tissues, at early stages of infection, can alter the course of disease in SIV infected macaques. In this regard $\alpha_4\beta_7$ mAb reduced virus in the colon to a greater extent that in the small bowel, which is consistent with the concept that immune tissues within the colon play a more central role in SIV pathogenesis.

At two and three weeks post infection $\alpha_4\beta_7$ mAb mediated reductions of viral antigen in GALT as expected, but also in lung, spleen, and inguinal and axillary lymph-nodes, none of which are known to constitutively express MAdCAM, the natural ligand for $\alpha_4\beta_7$. We speculate that, in the absence of $\alpha_4\beta_7$ mAb treatment, some of the virus that appears in these tissues reflects recirculation of infected $CD4^+$ T cells out of GALT. Thus, an initial reduction of viral antigen in GALT, mediated by $\alpha_4\beta_7$ mAb, could lead to corresponding reductions of viral antigen in these peripheral sites. As such, infection of GALT would, to a degree, function as a hub from which virus disseminates through a network of $\alpha_4\beta_7$ linked immune tissues. This suggestion represents a variation of the concept of a linked network of mucosal tissues [36, 37]. Of note, in each of our studies involving treatment with $\alpha_4\beta_7$ mAb during the acute phase of infection, plasma viral loads were reduced by only ~1log. This modest effect on plasma viremia is consistent with viral replication occurring outside an $\alpha_4\beta_7$ linked network as well. However, because $\alpha_4\beta_7$ mAb treatment promotes the preservation of $CD4^+$ T cells (Figure 5) and overall disease progression [20], viral replication within tissues linked by $\alpha_4\beta_7$ appears to play a more important role in SIV (and possibly HIV) pathogenesis.

An alternative explanation for $\alpha_4\beta_7$ mAb -mediated reductions of viral antigen in lung, spleen, and inguinal and axillary lymph-nodes involves dynamic aspects of MAdCAM expression. Although MAdCAM expression in mice has been well-characterized, less is known with respect to primates. Tissue specific expression of MAdCAM in humans is not restricted to the gut in newborns [38]. Several infectious agents that elicit inflammatory responses induce MAdCAM expression in adults outside of the gut. MAdCAM is expressed in the liver of hepatitis C infected individuals[39, 40], and the female genital tract of chlamydia-infected women[41, 42]. It is not known whether HIV and SIV upregulate MAdCAM. If that occurs, then it is possible that the $\alpha_4\beta_7$ mAb -mediated reductions of viral antigen outside of gut reflect a disruption of MAdCAM mediated homing to these tissues. In any case, these results underscore an important role for MAdCAM -$\alpha_4\beta_7$ interactions in the acute phase of SIV infection.

By the early-chronic phase, $\alpha_4\beta_7$ mAb reduced gp120 signals in the large intestine to a greater extent than in the small bowel. Notably, immune cells of the small bowel populate organized inductive sites while the large bowel is comprised primarily of effector sites [43, 44]. Our results are consistent with the hypothesis that protecting these GALT effector sites underlies the capacity of $\alpha_4\beta_7$ mAb treatment to slow the rate of disease progression in SIV infected macaques[20, 24]. In fact, colon biopsies taken more than 45 weeks PI showed significant preservation of $CD4^+$ T cells (Figure 5).

Although we can observe $\alpha_4\beta_7$ mAb-mediated reductions of virus in GALT by both PET/CT imaging (gp120) and PCR (pro-viral DNA), our analysis does not allow us to determine whether $\alpha_4\beta_7$ mAb is blocking access of infected $\alpha_4\beta_7^+/CD4^+$ cells to gut tissue, or alternatively, preventing uninfected $\alpha_4\beta_7^+/CD4^+$ cells from entering gut tissues where they serve as fresh targets for infection. In either instance the capacity of $\alpha_4\beta_7$ mAb to reduce gp120 signals, not just in GALT, but also in other lymphoid tissues provides compelling evidence that $\alpha_4\beta_7$ expressing cells play a central role in viral replication and spread.

SIV infected macaques treated with a combination of $\alpha_4\beta_7$ mAb and ART were able to control viremia in a durable way following treatment interruption. The immune mediators of virus control in those animals likely originated either during the dual-therapy phase of the treatment regimen, when animals were aviremic, or just afterward. By acquiring PET/CT images near the end of the dual-therapy period we are now able to report that aviremic animals receiving $\alpha_4\beta_7$ mAb exhibited lower levels of viral antigen (gp120) in tissues than animals receiving ART + IgG. Differences were most apparent in the large intestine, suggesting that the immune responses responsible for sustained control in these animals following ART interruption were linked with a reduction of viral antigen in the large intestine. There are several mechanisms that could explain how $\alpha_4\beta_7$ mAb treatment reduced viral antigen signals in the large intestine beyond the reduction mediated by ART + IgG. Unlike the studies in which $\alpha_4\beta_7$ mAb was employed w/o ART, the reduced gp120 signals in this instance occurred after 9 weeks of ART when the number of productively infected $CD4^+$ T cells (including those expressing $\alpha_4\beta_7$) was limited and thus their potential to home to GALT was low.

We conclude that is unlikely that the reduced signals reflect interference with trafficking of productively infected cells into GALT. Several alternative explanations remain. $\alpha_4\beta_7$ mAb may have reduced low-level viral replication within GALT in a direct way. Or it may have reduced the homing of uninfected $\alpha_4\beta_7$ expressing $CD4^+$ T cells to the large intestine. This also assumes ongoing viral replication in GALT. Other explanations involving homeostatic proliferation of infected cells in GALT may also be in play. Whichever mechanism explains these reduced gp120 signals, it is clear from week 23 $CD4^+$ cell imaging (Figure 8), that $\alpha_4\beta_7$ mAb promoted higher CD4 cell numbers not just in the large intestine but in other tissues as well. This supports the hypothesis that the $\alpha_4\beta_7$ mAb mediated reduction of virus in the large intestine during the dual-therapy treatment may contribute to preservation of lymphoid tissues throughout the body.

Pre-treatment with $\alpha_4\beta_7$ mAb alone failed to prevent the apparent depletion of $CD4^+$ cells in GALT during the acute phase of infection (Figures 4 and 5). This was surprising given its

capacity to reduce pro-viral DNA in the gut during acute infection (Figure 2). We confirmed this result by flow-cytometric analysis of colon biopsies, which showed similar levels of $CD4^+$ T cell reduction in IgG controls and $\alpha_4\beta_7$ mAb treated animals. This raises the possibility that some fraction of the $CD4^+$ T cell reduction that is typically observed in acute infection is not due to direct killing but rather to a redistribution of $CD4^+$ T cells away from GALT, possibly in response to inflammation. By early-chronic infection (weeks 12–15) the positive impact of $\alpha_4\beta_7$ mAb became evident, such that the $\alpha_4\beta_7$ mAb-treated animals were able to preserve a significant fraction of $CD4^+$ T cells, while these cells were almost entirely absent from IgG-treated control animals. Remarkably, this apparent preservation of the gut $CD4^+$ T cell compartment in viremic animals persisted well into chronic infection (after week 45) despite the fact that the last dose of mAb was administered around week 3. In this regard $\alpha_4\beta_7$ mAb therapy may serve to diminish the deterioration of GALT ultrastructure that occurs in the context of acute and chronic SIV/HIV infection. The preservation of GALT integrity could then provide an environment that minimizes the loss of $CD4^+$ T cells. These observations support the hypothesis that the profound destruction of GALT during acute infection is a key event in the development of immune deficiencies over time [2, 3, 4, 45, 46].

The mechanism by which $\alpha_4\beta_7$ mAb suppresses virus and protects $CD4^+$ cells in the gut remains elusive. The capacity of $\alpha_4\beta_7$ mAb to reduce viral antigen in tissues not associated with MAdCAM expression might suggest that interference with gp120- $\alpha_4\beta_7$ interactions underlie these reductions. However, as noted above, recirculation of infected cells from GALT to distal tissues and/or MAdCAM expression outside of gut may provide an explanation for this observation. Because $\alpha_4\beta_7$ mAb blocks both trafficking via MAdCAM-$\alpha_4\beta_7$ adhesion, and the interaction between $\alpha_4\beta_7$ and the SIV gp120s used in these studies, our experimental design does not allow us to differentiate between these mechanisms of action. Other mechanisms also need to be considered. $\alpha_4\beta_7$ is expressed on other lymphocytes including B cells and $CD8^+$ T cells and some dendritic cells and macrophages. $\alpha_4\beta_7$ mAb may impact these cells in a way that suppresses $CD4^+$ T cell infection. $\alpha_4\beta_7$ can appear on the surface of SIV virions [17, 47] and it is possible that $\alpha_4\beta_7$ mAb engages these virions. Finally, $\alpha_4\beta_7$ is a signal-transducing receptor which has the capacity to modulate the metabolic state of lymphocytes as they traffic into gut tissues [17, 27, 48]. $\alpha_4\beta_7$ mAb is likely to block signals delivered by MAdCAM and/or gp120 in a way that could suppress viral replication.

In summary, using a powerful new immuno-PET/CT imaging technique we show that $\alpha_4\beta_7$ mAb treatment, alone or combined with ART, impacts viral replication in a tissue and organ specific manner. While reductions in viral load mediated by $\alpha_4\beta_7$ mAb were apparent in gut tissues, we also observed reductions in tissues that are not typically associated with $\alpha_4\beta_7$-mediated homing. Imaging $CD4^+$ cells in uninfected macaques treated with $\alpha_4\beta_7$ mAb revealed that this treatment did not grossly deplete the complement of $CD4^+$ cells in gut tissues, indicating that its capacity to protect gut tissue from SIV cannot be explained simply as a consequence of the removal of $CD4^+$ T cells. To the contrary, $\alpha_4\beta_7$ mAb treatment appeared to promote the preservation of the $CD4^+$ T cell compartment in the gut, even in the face of ongoing plasma viremia. These observations, along with the fact that we have found no evidence that this antibody suppresses the immune system in an overt way, lead us to

conclude that $\alpha_4\beta_7$ mAb treatment provides an effective approach toward better defining the role of GALT infection and gut damage in SIV and HIV pathogenesis.

Materials and Methods

Ethics Statement

The animals from which blood samples and tissues were obtained utilized in the present study were born and maintained at the Yerkes National Primate Research Center (YNPRC) of Emory University, Atlanta, Georgia, USA. Their maintenance was performed in accordance with the rules and regulations of the Committee on the Care and Use of Laboratory Animal Resources. The animals were fed a monkey diet (Purina, Gray Summit, MO) supplemented daily with fresh fruit and/or vegetables and water ad libitum. Additional social enrichment including the delivery of appropriate safe toys were provided and overseen by the Yerkes enrichment staff and animal health was monitored daily and recorded by the animal care staff and veterinary personnel, available 24/7. Monkeys were caged in socially compatible same sex pairs to facilitate social enhancement and well-being. Monkeys showing signs of sustained weight loss, disease or distress were subject to clinical diagnosis based on symptoms and then provided either standard dietary supplementation analgesics and/or chemotherapy. Monkeys with sustained weight loss whose symptoms could not be alleviated using standard dietary supplementation, analgesics and/or chemotherapy were humanely euthanized using an overdose of barbiturates according to the guidelines of the American Veterinary Medical Association. The entire studies reported herein were performed under IACUC protocol #2001725-042715GA “Gut Homing Cells in SIV Infection” which was reviewed and approved by the Emory University IACUC. The YNPRC has been fully accredited by the Association for Assessment and Accreditation of Laboratory Animal Care International since 1985. In addition, all experiments were reviewed and approved by the Emory biosafety review Committee prior to initiation of the studies.

Animals and Sources of Virus and Blood & Tissue Samples

Juvenile to adult male and female rhesus macaques (*Macaca mulatta*) of Indian origin were used for the studies reported herein. The animals were all housed at the Yerkes National Primate Research Center (YNPRC) of Emory University (Atlanta, GA) and were maintained according to the guidelines of the Committee on the Care and Use of Laboratory Animals of the Institute of Laboratory Animal Resources, National Research Council and the Department of Health and Human Service guideline titled Guide for the Care and Use of Laboratory Animals. All studies were reviewed and approved by the Emory University IACUC.

The studies included animals a) that were infected with SIV mac251 or SIV mac239 and utilized for immuno-PET/CT imaging of SIV gp120 and $CD4^+$ cells during acute (<4 weeks) infection, are referred to as the “acute infection cohort”. Detailed methods are published elsewhere [24, 49]. b) Animals infected with SIV mac251 and utilized for immuno-PET/CT imaging of SIV and $CD4^+$ cells during early-chronic infection (16–17 weeks) are detailed elsewhere [20]. c) Animals treated with a combination of ART and $\alpha_4\beta_7$ mAb and

utilized for immuno-PET/CT imaging of SIV gp120 and $CD4^+$ cells during (week 16), and following ART interruption (weeks 22, 23), are described in detail elsewhere [26]. Colorectal biopsies were obtained from animals in the acute and early-chronic cohorts at various time-points up to 60 weeks PI. Select animals from the two cohorts were euthanized for organ and tissue specific viral load determination. The SIV mac251 stock virus was supplied by the NIAID Division of AIDS (Dr. Nancy Miller). SIV mac239 stocks were prepared as described elsewhere [24, 50]. Supplementary Table 1 summarizes the details of the animals that were subject to PET/CT image analysis for SIV and $CD4^+$ cells including route of SIV infection, stage of infection, time of imaging, plasma viral load and CD4 count at the time of analysis. Supplementary Figure 1 summarizes $\alpha_4\beta_7$ mAb and the timeline of image acquisition.

Animals from the acute infection animals received either 50 mg/kg of a “primatized” recombinant $\alpha_4\beta_7$ mAb or 50 mg/kg of normal recombinant rhesus IgG intravenously on day-3 and day 21. On day 0, each of these animals was infected intra-rectally with either 500 TCID50 of a stock of SIV mac251 or 200 TCID50 of SIVmac239 intravenously as previously described [20]. The animals in the acute infection were subjected to immuno-PET/CT imaging of SIV and $CD4^+$ cells during week 2 and the same animals from each group subjected to immuno-PET/CT imaging of SIV gp120 and $CD4^+$ cells during week 3. Tissues were collected from each of these animals at autopsy. Blood samples were collected in EDTA prior to infection (baseline) and weekly post infection until the termination of the study. GALT biopsies were also obtained prior to infection (baseline) and at 2 and 4 weeks post infection.

Two groups of SIV infected rhesus macaques comprised the early-chronic infection animals. One group of animals received 50 mg/kg of the “primatized” recombinant $\alpha_4\beta_7$ mAb and the other group of three received 50 mg/kg of normal recombinant rhesus IgG intravenously on day −3 and the same dose every 3 weeks for the duration of their study. On day 0, each of these animals was infected intra-rectally with 500 $TCID_{50}$ of a stock of SIV mac251 or 200 $TCID_{50}$ of SIV mac239 intravenously. The stocks we utilized for these studies has been reported previously [24, 49]. Animals were subjected to immuno-PET/CT imaging for SIV gp120 during chronic infection. Blood samples in EDTA were obtained from each of these monkeys prior to infection (baseline), and weekly for the first 6 weeks, bi-weekly for another 4 weeks and then at monthly intervals thereafter. GALT biopsies were obtained prior to infection (baseline) and at 2, 4, 6 and 8 weeks and monthly thereafter. Aliquots of the plasma samples and GALT biopsies were subjected to viral and pro-viral load determinations as previously described [20].

At autopsy >20 different tissues were obtained from each animal for quantitation of tissue specific viral loads and included lymph-nodes (regional inguinal, regional axillary, cervical, mesenteric, external and internal iliac), heart, spleen, liver, lung, tonsils, jejunum, colon, ileum, bone marrow and muscle. In addition, from the males, prostate, seminal vesicles, and penis tissues and from the females, uterus, vaginal, ovaries, cervix, and fallopian tissues were obtained.

Viral load determinations

Plasma viral loads were carried out on EDTA containing plasma using an established qRT-PCR technique [20]. The sensitivity of the assays was 50 copies/ml of plasma. Tissue pro-viral DNA loads were performed on DNA extracts also as previously described [20] and the sensitivity of the assay was 0.1 copy/ng of DNA. Appropriate controls were included with each assay.

$CD4^+$ T-cell counts

The values for absolute numbers of $CD4^+$ T cells were determined as described previously[20]. In brief, the PBMCs were isolated from EDTA/heparin blood and an aliquot stained with Alexa700 CD3; PerCP-Cy5.5 CD4 antibodies and analyzed using a LSR-Fortessa flow cytometer (B-D Immunocytometry Division, Mountain View, CA). The CBC values were then utilized to calculate the absolute number of $CD4^+$ T cells.

In vivo administration of imaging probes antibodies and imaging methodology

A large number of anti-SIV env and anti-CD4 monoclonal antibodies (mAb) were first screened and optimal clones were chosen for the studies reported herein. In the case of screening for SIV reactivity, the screening included staining for virus infected cells in the presence of normal rhesus plasma and plasma from an SIV infected rhesus macaque. For the in vivo imaging of gp20 we utilized the mAb (clone 7D3) that has been characterized previously [28]. mAb 7D3 is a non-neturalizing high affinity anti SIV gp120 antibody. For the imaging of CD4 expressing cells we utilized a “primatized” $F(ab')_2$ monoclonal antibody (clone OKT4A). Both the OKT4A and the isotype control antibody utilized in parallel were obtained from the NIH Non-human Primate Reagent Resource, Boston, MA. Imaging mAbs were covalently modified by polyethylene glycol and DOTA NHS or only DOTA NHS as previously described [51] and kept lyophilized until use. The lyophilized antibodies were re-suspended in chelexed 0.1M NH_4OAc pH 5.5 (Sigma-Aldrich) as was the Copper (II)-64 chloride Washington University, St. Louis, MO) and the two mixed at a ratio of approximately 5 mCi/mg of protein and incubated for 1 hr at 37C. The radio-labeled probes were dialyzed X 3 with pharmaceutical grade saline and concentrated using a centrifugation filter to a volume of 20ul. A small aliquot was utilized for confirmation of uptake using thin layer chromatography. The conjugated antibody gave values between 1 to 3.5 mCi/mg protein. The animal to be imaged was administered the ^{64}Cu-labeled antibody intravenously in a volume of 3 ml of sterile saline and the animal placed in a separate holding room. Approximately 24 to 48 hr later the animal was sedated with Telazol ketamine (5 mg/kg intramuscular) and transported to the PET-CT imaging facility located at Emory University Clinic. Anesthesia was maintained by supplementing with Ketamine as needed. The animals were imaged using a Siemens Biograph 40 PET/CT that was adjusted for settings optimal for ^{64}Cu. Between 250–300 image slices were compiled for each animal.

Immuno-PET/CT image analysis

Images from the PET/CT fusions were analyzed utilizing the OsiriX software. The Region of Interest (ROI) tool was used to measure maximum and Mean Standard Uptake Value (SUVmaxwithin a specific organ or tissue. The SUVmax value reflects the density of the

highest signal obtained within a tissue or organ and the SUVMean reflects the Mean of the signals obtained within an ROI that covers the entire tissue or organ. Details of these analyses have been published elsewhere [28]. Values obtained using the PET/CT methodology, gp120 SUVmax values were validated by comparison with levels of SIV as determined by quantitative PCR of the same tissues (quantitative PCR CD4 signals were also included) (Supplementary Figure 7) as previously described[28]. Both SUVmax values and quantitative PCR measurements across both acute and early-chronic cohorts were pooled. Values from IgG-treated animals in these same cohorts were also plotted.

Immuno-PET/CT CD4 Specificity and Sensitivity Determination

Anti-CD4 F(ab′)$_2$ was reacted with a 6× molar excess of Dylight 650 NHS Ester (Thermo Fisher Scientific) for 1 hour under constant shaking at room temperature. The average number of Dylight 650 molecules per F(ab′)$_2$ was 1.2, as determined via spectrophotometer. Retention of binding ability after labelling was confirmed using rhesus macaque PBMCs via flow cytometry. Each monkey was intravenously injected simultaneously with 1mg of anti-CD4 F(ab′)$_2$ labeled with DOTA and ^{64}Cu and 1 mg of anti-CD4 F(ab′)$_2$ labeled with Dylight 650, in 300μL of saline. After PET/CT imaging at 36 hours post injection, the animals were sacrificed. Primary and secondary lymphatic organs were resected and weighed. Spleen and lymph node preparations were mechanically dissociated into single cell suspensions and cells numbers quantified via hemocytometer. The gating scheme for CD3 + T cells was as follows: lymphocyte selection through FSC-A vs SSC-A gating, single cell selection through FSC-A vs FSC-H gating, and T cell selection through CD3 gating using anti-CD3 clone SP34-2 (BD Biosciences). To verify the specificity of our injected probe for CD4 positive T cells, anti-CD4 clone L200 (BD Biosciences) confirmatory staining was used to identify CD4 + cells *in vitro.* L200 was used for staining as it binds to a different epitope than our OKT4 derived F(ab′)$_2$ imaging probes. The percentage of CD3+/CD4+ cells based on L200 staining and Dylight 650 labelled imaging probe uptake, respectively, was reported for each organ. All samples were acquired using a FACS Aria Fusion cell sorter equipped with 405, 488, and 640 laser lines (BD Biosciences). All analysis was performed using the FlowJo software package (Tree Star, Ashland, OR, USA). A total of at least 500,000 events were recorded for each organ.

Statistical Analyses

Statistical significance for Figures 1 and 5 was assessed utilizing the two-tailed unpaired Student's t-test for multiple comparisons. The Wilcoxon rank sum test was used to compare study group differences. Mixed effects regression models were implemented to test for group differences and trends using lonGALTudinal, repeated measurements. Reported *p*-values are based on two-sided testing and a *p*-value <0.05 was considered statistically significant. Statistical analyses were performed using Prism® GraphPad Software (version 5, CA) or SAS software, version 9.3 (SAS Institute, Cary, NC, USA). The values for $p < 0.05$ is represented by *, $p< 0.001$ is represented by ** and $p < 0.0001$ is represented by ***. For Figures 2, 4, and 6–8, The open source R statistical package was utilized for estimation and hypothesis testing at a significance level of 0.05. For analysis of SIV and CD4 immunoPET SUVmax comparisons, a repeated measures ANOVA with organ and treatment type as the factors was performed. NHPs were grouped during hypothesis testing and not

analyzed individually due to low sample numbers. Confidence Interval estimation was used to evaluate which organs contributed the most to the observed variation between treatment groups.

Supplementary Material

Refer to Web version on PubMed Central for supplementary material.

Acknowledgments

The authors are grateful to the veterinary staff of the Yerkes National Primate Research Center of Emory University specially Ms. Stephanie Ehnert and her supporting staff members for coordinating all the nonhuman primate work. In addition, the authors are grateful to Dr. D. M. Schuster and the technical staff of the Department of Imaging Sciences and Radiology of Emory University Hospital, Emory University School of Medicine for their help and guidance for the imaging studies. The authors also would like to thank Dr. James Hoxie for the provision of the 7D3 hybridoma, Dr. K. Reimann and Mr. Adam Busby for the provision of primatized $\alpha_4\beta_7$ mAb, the normal recombinant rhesus IgG and the anti-CD4 $(Fab)_2$. We are also grateful to E. Husband and his colleagues at the Emory hospital imaging facility for scanning the animals, Drs. S. Jean, J. Wood, F Connor-Stroud and the Yerkes Veterinary and animal care team for their support of these studies. Finally, we are grateful to Alia Sanjani for editorial assistance.

Funding: This work is supported by NIH R01 AI098628 to A. A. A., the Intramural Research Program, NIAID, NIH, Bethesda, MD and NIH R01 AI111907 to P.J.S and FV. Anti $\alpha_4\beta_7$ mAb, rhesus IgG mAb and anti-CD4 $(Fab)_2$ provided by the NIH Nonhuman Primate Reagents Resource supported by AI126683 and OD010976.

References

1. Guadalupe M, et al. Severe CD4+ T-cell depletion in gut lymphoid tissue during primary human immunodeficiency virus type 1 infection and substantial delay in restoration following highly active antiretroviral therapy. J Virol. 2003; 77:11708–11717. [PubMed: 14557656]
2. Heise C, Miller CJ, Lackner A, Dandekar S. Primary acute simian immunodeficiency virus infection of intestinal lymphoid tissue is associated with gastrointestinal dysfunction. J Infect Dis. 1994; 169:1116–1120. [PubMed: 8169404]
3. Mehandru S, et al. Primary HIV-1 infection is associated with preferential depletion of CD4+ T lymphocytes from effector sites in the gastrointestinal tract. J Exp Med. 2004; 200:761–770. [PubMed: 15365095]
4. Veazey RS, et al. Gastrointestinal tract as a major site of CD4+ T cell depletion and viral replication in SIV infection. Science. 1998; 280:427–431. [PubMed: 9545219]
5. Brenchley JM, et al. CD4+ T cell depletion during all stages of HIV disease occurs predominantly in the gastrointestinal tract. J Exp Med. 2004; 200:749–759. [PubMed: 15365096]
6. George MD, Reay E, Sankaran S, Dandekar S. Early antiretroviral therapy for simian immunodeficiency virus infection leads to mucosal CD4+ T-cell restoration and enhanced gene expression regulating mucosal repair and regeneration. J Virol. 2005; 79:2709–2719. [PubMed: 15708990]
7. Kader M, et al. Antiretroviral therapy prior to acute viral replication preserves CD4 T cells in the periphery but not in rectal mucosa during acute simian immunodeficiency virus infection. J Virol. 2008; 82:11467–11471. [PubMed: 18768962]
8. Lifson JD, et al. Transient early post-inoculation anti-retroviral treatment facilitates controlled infection with sparing of CD4+ T cells in gut-associated lymphoid tissues in SIVmac239-infected rhesus macaques, but not resistance to rechallenge. J Med Primatol. 2003; 32:201–210. [PubMed: 14498980]
9. Verhoeven D, Sankaran S, Dandekar S. Simian immunodeficiency virus infection induces severe loss of intestinal central memory T cells which impairs CD4+ T-cell restoration during antiretroviral therapy. J Med Primatol. 2007; 36:219–227. [PubMed: 17669210]

10. Yukl SA, et al. The distribution of HIV DNA and RNA in cell subsets differs in gut and blood of HIV-positive patients on ART: implications for viral persistence. J Infect Dis. 2013; 208:1212–1220. [PubMed: 23852128]
11. Estes JD, et al. Antifibrotic therapy in simian immunodeficiency virus infection preserves CD4+ T-cell populations and improves immune reconstitution with antiretroviral therapy. J Infect Dis. 2015; 211:744–754. [PubMed: 25246534]
12. Paiardini M, Muller-Trutwin M. HIV-associated chronic immune activation. Immunol Rev. 2013; 254:78–101. [PubMed: 23772616]
13. Hearps AC, Martin GE, Rajasuriar R, Crowe SM. Inflammatory co-morbidities in HIV+ individuals: learning lessons from healthy ageing. Curr HIV/AIDS Rep. 2014; 11:20–34. [PubMed: 24414166]
14. Okoye AA, Picker LJ. CD4(+) T-cell depletion in HIV infection: mechanisms of immunological failure. Immunol Rev. 2013; 254:54–64. [PubMed: 23772614]
15. Talal AH, et al. Virologic and immunologic effect of antiretroviral therapy on HIV-1 in gut-associated lymphoid tissue. J Acquir Immune Defic Syndr. 2001; 26:1–7. [PubMed: 11176263]
16. Berlin C, et al. Alpha 4 beta 7 integrin mediates lymphocyte binding to the mucosal vascular addressin MAdCAM-1. Cell. 1993; 74:185–195. [PubMed: 7687523]
17. Cicala C, et al. The integrin alpha4beta7 forms a complex with cell-surface CD4 and defines a T-cell subset that is highly susceptible to infection by HIV-1. Proc Natl Acad Sci U S A. 2009; 106:20877–20882. [PubMed: 19933330]
18. Kader M, et al. Alpha4(+)beta7(hi)CD4(+) memory T cells harbor most Th-17 cells and are preferentially infected during acute SIV infection. Mucosal Immunol. 2009; 2:439–449. [PubMed: 19571800]
19. Martinelli E, et al. The frequency of alpha(4)beta(7)(high) memory CD4(+) T cells correlates with susceptibility to rectal simian immunodeficiency virus infection. J Acquir Immune Defic Syndr. 2013; 64:325–331. [PubMed: 23797688]
20. Byrareddy SN, et al. Targeting alpha4beta7 integrin reduces mucosal transmission of simian immunodeficiency virus and protects gut-associated lymphoid tissue from infection. Nat Med. 2014; 20:1397–1400. [PubMed: 25419708]
21. Byrareddy SN, et al. Species-specific differences in the expression and regulation of alpha4beta7 integrin in various nonhuman primates. J Immunol. 2015; 194:5968–5979. [PubMed: 25948815]
22. Habtezion A, Nguyen LP, Hadeiba H, Butcher EC. Leukocyte Trafficking to the Small Intestine and Colon. Gastroenterology. 2015
23. Pereira LE, et al. Preliminary in vivo efficacy studies of a recombinant rhesus anti-alpha(4)beta(7) monoclonal antibody. Cell Immunol. 2009; 259:165–176. [PubMed: 19616201]
24. Ansari AA, et al. Blocking of alpha4beta7 gut-homing integrin during acute infection leads to decreased plasma and gastrointestinal tissue viral loads in simian immunodeficiency virus-infected rhesus macaques. J Immunol. 2011; 186:1044–1059. [PubMed: 21149598]
25. Kwa S, et al. Plasmacytoid dendritic cells are recruited to the colorectum and contribute to immune activation during pathogenic SIV infection in rhesus macaques. Blood. 2011; 118:2763–2773. [PubMed: 21693759]
26. Byrareddy SN, et al. Sustained virologic control in SIV+ macaques after antiretroviral and alpha4beta7 antibody therapy. Science. 2016; 354:197–202. [PubMed: 27738167]
27. Arthos J, et al. HIV-1 envelope protein binds to and signals through integrin alpha4beta7, the gut mucosal homing receptor for peripheral T cells. Nat Immunol. 2008; 9:301–309. [PubMed: 18264102]
28. Santangelo PJ, et al. Whole-body immunoPET reveals active SIV dynamics in viremic and antiretroviral therapy-treated macaques. Nat Methods. 2015; 12:427–432. [PubMed: 25751144]
29. Sigmundsdottir H, Butcher EC. Environmental cues, dendritic cells and the programming of tissue-selective lymphocyte trafficking. Nat Immunol. 2008; 9:981–987. [PubMed: 18711435]
30. Stenstad H, et al. Gut-associated lymphoid tissue-primed CD4+ T cells display CCR9-dependent and -independent homing to the small intestine. Blood. 2006; 107:3447–3454. [PubMed: 16391017]

31. Couedel-Courteille A, et al. Delayed viral replication and CD4(+) T cell depletion in the rectosigmoid mucosa of macaques during primary rectal SIV infection. Virology. 2003; 316:290–301. [PubMed: 14644611]
32. Engelhardt B, Briskin MJ. Therapeutic targeting of alpha 4-integrins in chronic inflammatory diseases: tipping the scales of risk towards benefit? Eur J Immunol. 2005; 35:2268–2273. [PubMed: 16052610]
33. Feagan BG, et al. Vedolizumab as induction and maintenance therapy for ulcerative colitis. N Engl J Med. 2013; 369:699–710. [PubMed: 23964932]
34. Jovani M, Danese S. Vedolizumab for the treatment of IBD: a selective therapeutic approach targeting pathogenic a4b7 cells. Curr Drug Targets. 2013; 14:1433–1443. [PubMed: 23980911]
35. Sandborn WJ, et al. Vedolizumab as induction and maintenance therapy for Crohn's disease. N Engl J Med. 2013; 369:711–721. [PubMed: 23964933]
36. Bienenstock J, McDermott M, Befus D, O'Neill M. A common mucosal immunologic system involving the bronchus, breast and bowel. Adv Exp Med Biol. 1978; 107:53–59. [PubMed: 742502]
37. Gill N, Wlodarska M, Finlay BB. The future of mucosal immunology: studying an integrated system-wide organ. Nat Immunol. 2010; 11:558–560. [PubMed: 20562837]
38. Salmi M, et al. Immune cell trafficking in uterus and early life is dominated by the mucosal addressin MAdCAM-1 in humans. Gastroenterology. 2001; 121:853–864. [PubMed: 11606499]
39. Grant AJ, Lalor PF, Hubscher SG, Briskin M, Adams DH. MAdCAM-1 expressed in chronic inflammatory liver disease supports mucosal lymphocyte adhesion to hepatic endothelium (MAdCAM-1 in chronic inflammatory liver disease). Hepatology. 2001; 33:1065–1072. [PubMed: 11343233]
40. Hillan KJ, et al. Expression of the mucosal vascular addressin, MAdCAM-1, in inflammatory liver disease. Liver. 1999; 19:509–518. [PubMed: 10661685]
41. Kelly KA, et al. Chlamydia trachomatis infection induces mucosal addressin cell adhesion molecule-1 and vascular cell adhesion molecule-1, providing an immunologic link between the fallopian tube and other mucosal tissues. J Infect Dis. 2001; 184:885–891. [PubMed: 11550128]
42. Kelly KA, et al. The combination of the gastrointestinal integrin (alpha4beta7) and selectin ligand enhances T-Cell migration to the reproductive tract during infection with Chlamydia trachomatis. Am J Reprod Immunol. 2009; 61:446–452. [PubMed: 19392980]
43. Houston SA, et al. The lymph nodes draining the small intestine and colon are anatomically separate and immunologically distinct. Mucosal Immunol. 2015
44. Mowat AM, Agace WW. Regional specialization within the intestinal immune system. Nat Rev Immunol. 2014; 14:667–685. [PubMed: 25234148]
45. Mattapallil JJ, et al. Massive infection and loss of memory CD4+ T cells in multiple tissues during acute SIV infection. Nature. 2005; 434:1093–1097. [PubMed: 15793563]
46. Brenchley JM, Douek DC. HIV infection and the gastrointestinal immune system. Mucosal Immunol. 2008; 1:23–30. [PubMed: 19079157]
47. Guzzo C II, Park C, Phillips D, Liu Q, Zhang P, Kwon A, Miao H, Rehm C, Arthos J, Cicala C, Cohen M, Fauci AS, Kehrl J, Lusso P. Virion incorporation of integrin alpha4beta7 facilitates HIV-1 infection and intestinal homing. Science Immunology. 2017
48. Lehnert K, Print CG, Yang Y, Krissansen GW. MAdCAM-1 costimulates T cell proliferation exclusively through integrin alpha4beta7, whereas VCAM-1 and CS-1 peptide use alpha4beta1: evidence for "remote" costimulation and induction of hyperresponsiveness to B7 molecules. Eur J Immunol. 1998; 28:3605–3615. [PubMed: 9842903]
49. Amara RR, et al. Control of a mucosal challenge and prevention of AIDS by a multiprotein DNA/MVA vaccine. Vaccine. 2002; 20:1949–1955. [PubMed: 11983252]
50. Kestler HW 3rd, et al. Importance of the nef gene for maintenance of high virus loads and for development of AIDS. Cell. 1991; 65:651–662. [PubMed: 2032289]
51. Edinger AL, et al. Characterization and epitope mapping of neutralizing monoclonal antibodies produced by immunization with oligomeric simian immunodeficiency virus envelope protein. J Virol. 2000; 74:7922–7935. [PubMed: 10933700]

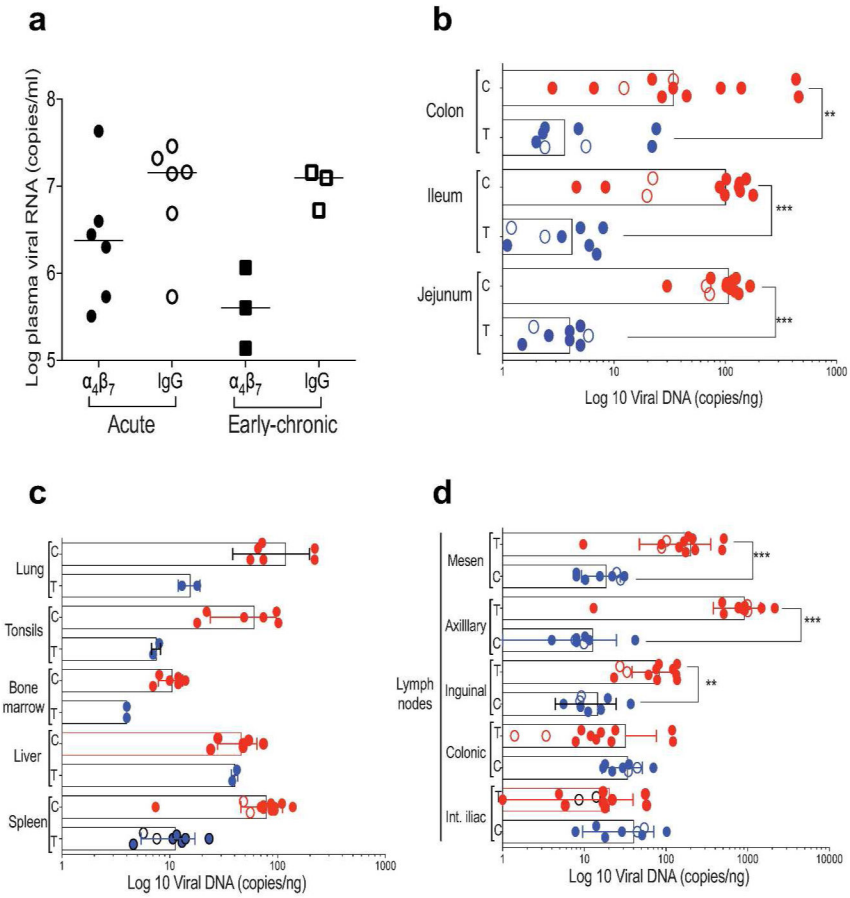

Figure 1. Plasma and tissue viral loads

(a) Peak plasma viral loads of acute and early-chronic cohorts are displayed. Included in this analysis were 6 animals from the acute cohort that received IgG (open circles) and 6 animals that received $\alpha_4\beta_7$ mAb (closed circles) IV at day −3 prior to infection. From the early-chronic cohort 3 animals that received IgG (open squares) and 3 animals that received $\alpha_4\beta_7$ mAb (closed squares), on day −3 and every 3 weeks until autopsy, were analyzed. **(b)** Pro-viral DNA levels in jejunum, ileum and colon tissues from $\alpha_4\beta_7$ mAb (T: $\alpha_4\beta_7$mAb treated), and IgG treated animals (C: control IgG treated) obtained at autopsy are displayed. Animals described in panel A, and additional animals treated in an identical manner are included. **(c)** Pro-viral DNA levels obtained from lymph-nodes of the internal iliac (Int. iliac), colonic, inguinal, axillary and mesenteric lymph-nodes from $\alpha_4\beta_7$ mAb (T: $\alpha_4\beta_7$ mAb), and IgG treated animals (C: IgG) at autopsy are displayed. **(d)** Pro-viral DNA in spleen, liver, bone marrow, tonsils and lung from $\alpha_4\beta_7$ mAb (T: $\alpha_4\beta_7$ mAb), and IgG treated animals (C: IgG) at autopsy are illustrated. For statistical analysis, data on tissues obtained during acute infection and early-chronic infection were pooled. Symbols * and ** represent p values of < 0.05 and < 0.01, respectively (Mann-Whitney *U*-test).

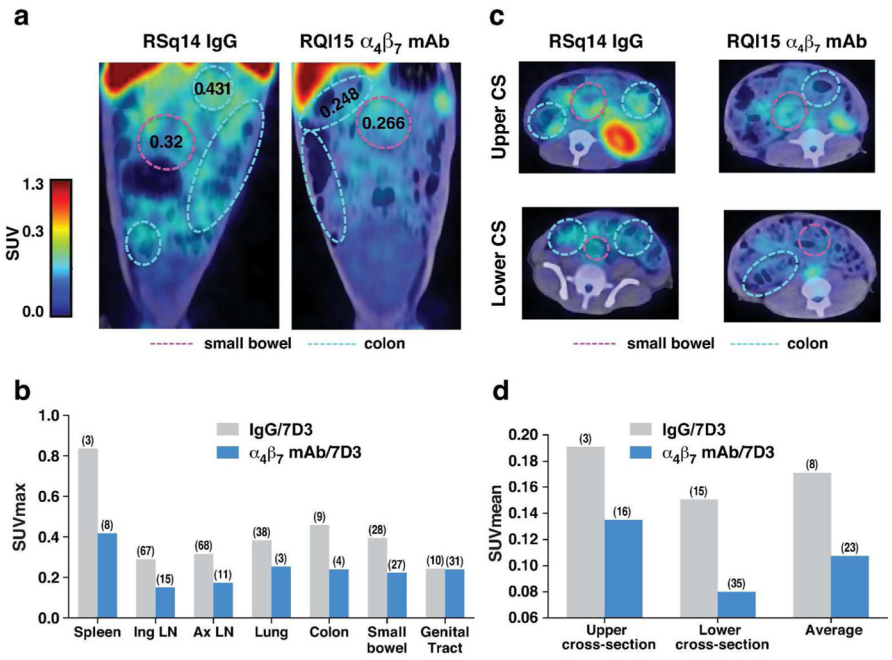

Figure 2. Tissue-specific localization of SIV gp120 during acute infection by Immuno-PET/CT image analysis

(a) Representative PET/CT imaging of the small bowel and colon of two macaques 3 weeks post-infection with ^{64}Cu/DOTA labeled, PEG conjugated SIV gp120 mAb clone 7D3. Animals were treated with either IgG (RSQ14) or $\alpha_4\beta_7$ mAb (RQL15). SUVmax values within defined regions of small bowel and colon are presented. **(b)** The average SUVmax values from two IgG treated (RSQ14, RPG15) and two $\alpha_4\beta_7$ mAb treated (RQL15, RPJ15) animals at 3 weeks post infection for the spleen, inguinal lymph-nodes (ING LN), axillary lymph-nodes (AX LN), lung, colon, small bowel, and genital tract. (**c)** Axial upper and lower cross-sectional Immuno-PET/CT images from RSQ14 (IgG) or RQL15 ($\alpha_4\beta_7$ mAb). SUVmax values within defined regions of small bowel and colon are presented. **(c)** The calculated SUVMean values from two IgG treated (RSQ14, RPG15) and two $\alpha_4\beta_7$ mAb treated (RQL15, RPJ15) animals at 3 weeks post infection for the upper and lower cross sectional axial images displayed in **c**, along with the combined averages for both upper and lower cross-sections. Median coefficient of variation (CV) indicated in parenthesis in panels b and d.

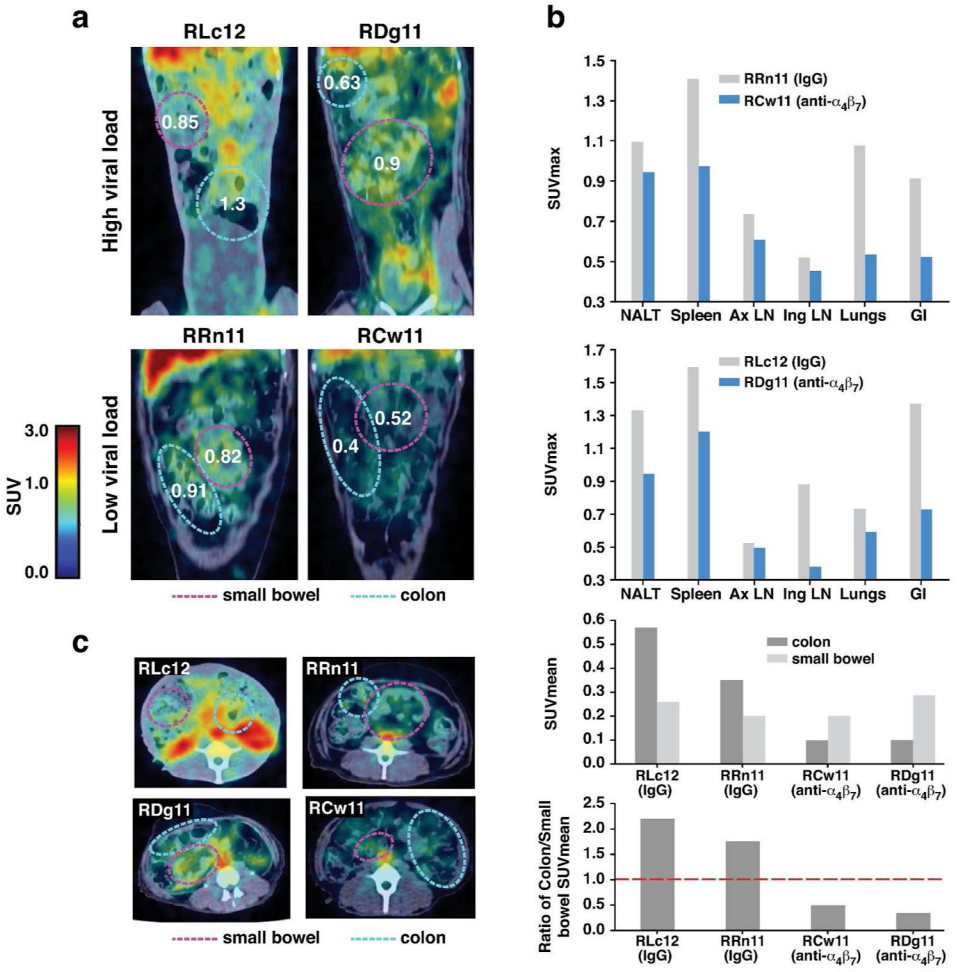

Figure 3. Tissue specific localization of SIV gp120 during early-chronic infection by immuno-PET/CT image analysis

PET/CT images of the small bowel and colon of 2 macaques (RLC12 and RRN11) that received IgG and 2 macaques that received $\alpha_4\beta_7$ mAb (RDG11 and RCW11) on day −3 and every 3 weeks thereafter until autopsy (weeks 16–17), with ^{64}Cu/DOTA labeled, PEG conjugated SIV gp120 mAb clone 7D3. (**a)** The immuno-PET/CT frontal images of the 4 macaques, with the small bowel and colon highlighted. (**b)** SUVmax values for nasal lymphoid tissues (NALT), spleen, axillary lymph-nodes (Ax LN), inguinal lymph-nodes (Ing LN), lungs and the gastro-intestinal tissues (GI) on RRN11 and RCW11 (left bar graph, low viral load) and RLC12 and RDG11 (right bar graph, high viral load). (**c)** Representative cross-sectional immuno-PET/CT images of SIV for the same 4 macaques is shown (top panel), along with the calculated SUVMean values for the colon and small bowel of the $\alpha_4\beta_7$ mAb (RDG11 and RCW11) and IgG treated (RLC12 and RRN11) animals (middle panel). The ratios of the SUVMean values for the colon versus the small bowel for each of the 4 animals are illustrated (bottom panel). The broken line indicates a ratio of 1.

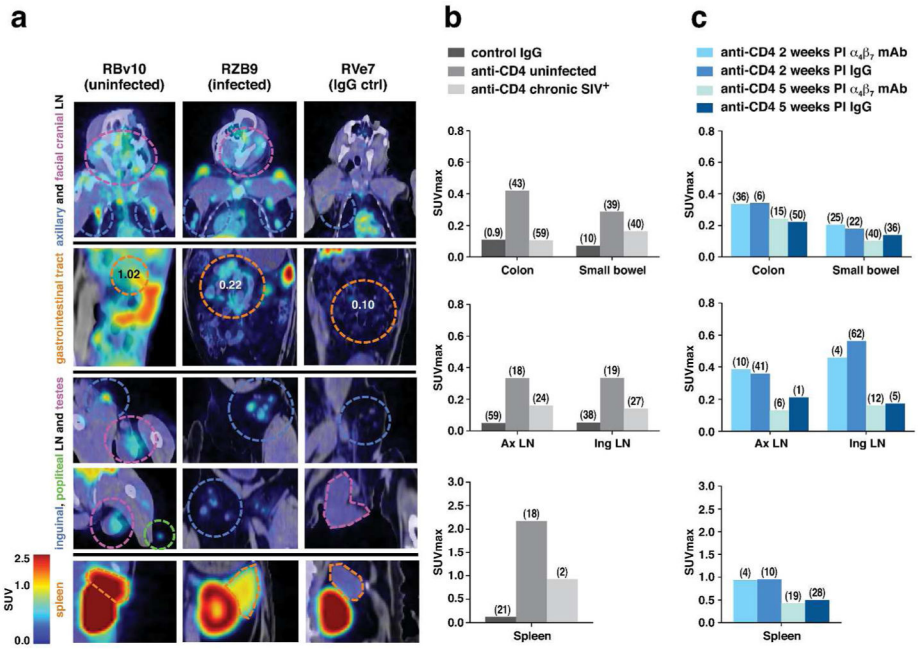

Figure 4. Immuno-PET/CT analysis of CD4$^+$ cells in uninfected, infected, and infected/mAb $\alpha_4\beta_7$ -treated macaques

(a) Representative immuno-PET/CT profiles of CD4$^+$ cells from various tissues in an uninfected animal (RBv10) and a chronically infected animal (RZB9) who both received ^{64}Cu-(Fab)$_2$ anti-CD4 mAb and an uninfected animal (RVe7) that received a ^{64}Cu-isotype IgG control mAb. Frontal images of axillary and facial cranial lymph-nodes, GI tract, inguinal and popliteal lymph-nodes, testes and spleen of all 4 macaques is designated by broken circles; color of each circle corresponds to the colored text (left). (**b)** SUVmax values for colon, small bowel, axillary (AxLN) and inguinal lymph-nodes (Ing LN), and spleen of 2 animals (RVe7, RHg7), probed with ^{64}Cu-isotype mAb, along with 4 uninfected (RVg13, RVg7, RWg13, RBg10) animals, and 2 SIV chronically infected animals. (**c)** SUVmax values of 2 acutely infected animals (RZB9, RTI12) treated with the $\alpha_4\beta_7$ mAb (ROe15, ROr14) at 2 and 5 weeks post-infection, and 2 acutely infected animals treated with IgG (RUp14, RVo14), imaged at 2 and 5 weeks PI probed with ^{64}Cu-(Fab)$_2$ anti-CD4 mAb. Median coefficient of variation (CV) indicated in parenthesis in panels b and c.

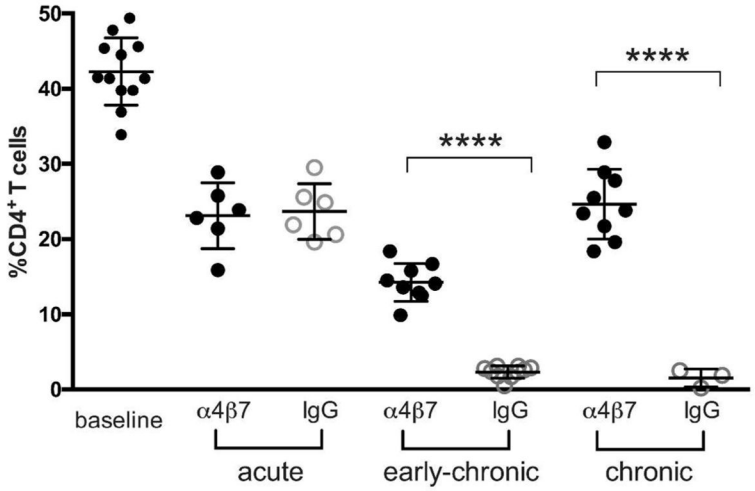

Figure 5. CD4$^+$ T cell frequencies in colorectal biopsies of $\alpha_4\beta_7$ mAb-treated macaques

Frequencies of CD4$^+$/CD45$^+$ cells derived from colorectal biopsies from acute (weeks 2–5), early-chronic (weeks 12–15), and chronic (after week 45) infected macaques treated with either $\alpha_4\beta_7$ mAb or IgG. Y-axis represents the frequency (%) of CD4$^+$/CD45$^+$ lymphocytes. Symbols **** represents p values of < 0.0001(unpaired t-test).

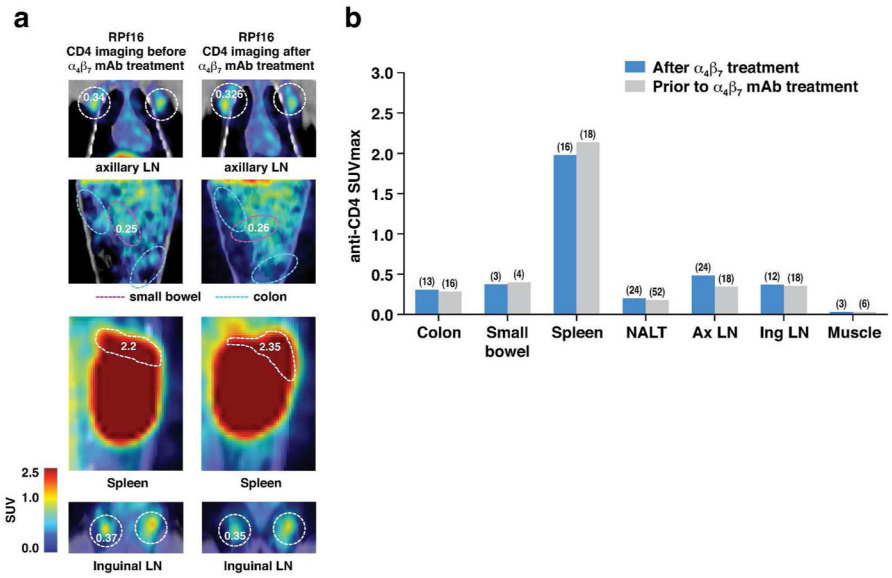

Figure 6. Immuno-PET imaging of CD4$^+$ cells in uninfected animals before and after $\alpha_4\beta_7$ mAb treatment

(a) Images of CD4$^+$ cell localization in a representative animal, RPF16, before and after treatment with $\alpha_4\beta_7$ mAb antibody. Designated tissues are outlined by dashed circles. SUVmax values are indicated before and after treatment. (**b)** Quantification of anti CD4 PET signals in various tissues in 4 animals before and after treatment with $\alpha_4\beta_7$ mAb. Median coefficient of variation (CV) indicated in parenthesis in panel b.

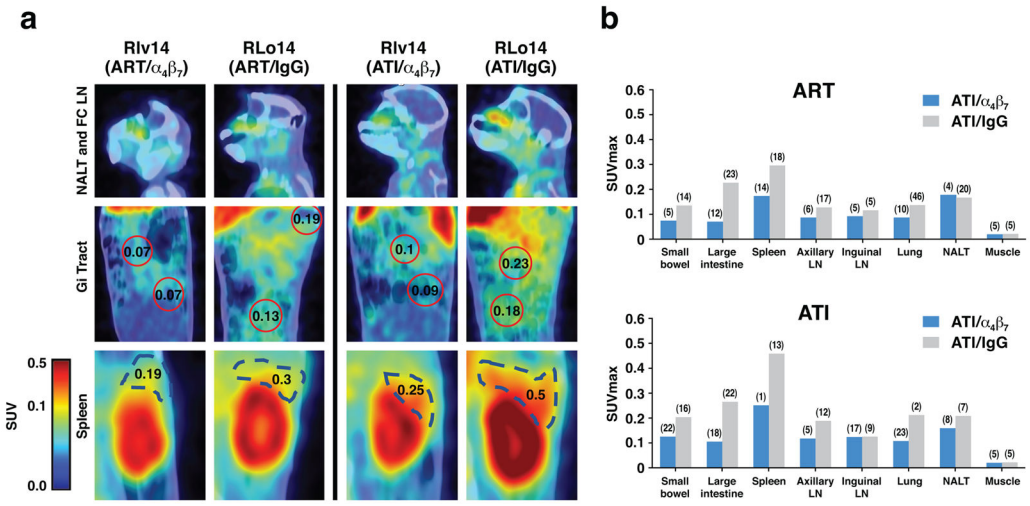

Figure 7. Immuno-PET/CT analysis of SIV gp120 in animals treated with ART+ $\alpha_4\beta_7$ dual-therapy

Comparison of gp120 signals in two ART + $\alpha_4\beta_7$ mAb treated animals and two ART-only animals at weeks 16 and 22. **(a)** Representative gp120 immuno-PET/CT images from NALT and facio-cranial LNs, GI tract and spleen of a macaque receiving dual-therapy (RIv14) or ART + IgG (RLo14) at weeks 16 (left panels) and 22 (right panels). Selected SUVmax values within the GI tract and spleen are displayed. **(b)** Average SUVmax values in selected tissues from two animals treated with dual-therapy (ROq14, RIv14)(cyan) and two animals treated with ART+ control IgG (RLo14 and RUs14)(magenta) at weeks 16 during dual therapy (upper panel), and week 22, 4 weeks after ART interruption (lower panel). Median coefficient of variation (CV) indicated in parenthesis in panel b.

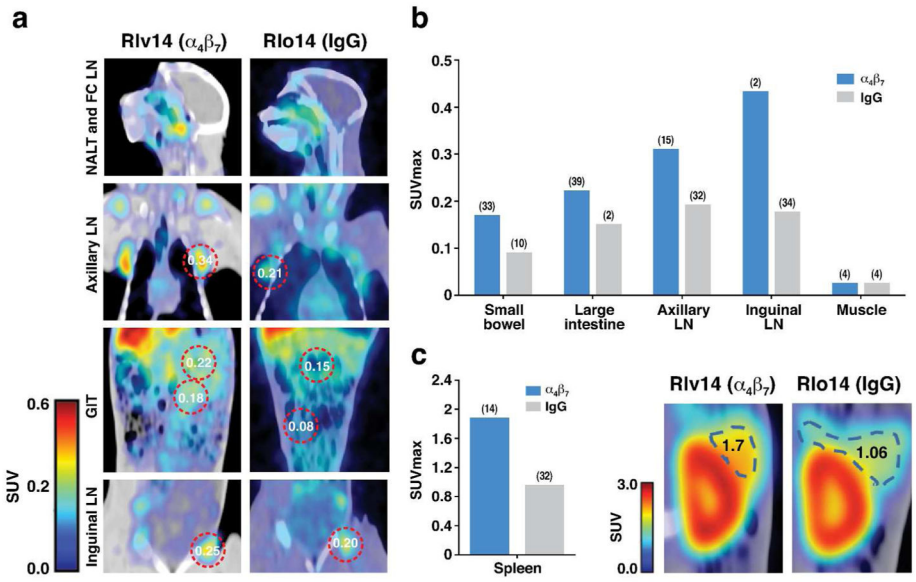

Figure 8. Immuno-PET/CT analysis of CD4$^+$ cells in animals treated with ART+ $\alpha_4\beta_7$ dual-therapy

Comparison of CD4$^+$ cell signals in two ART + $\alpha_4\beta_7$ mAb treated animals and two ART-only animals at weeks 16 and 22. **(a)** Representative CD4$^+$ cell immuno-PET/CT images from selected tissues of a macaque receiving dual-therapy (RIv14) or ART + control IgG (RLo14) at week 23. Selected SUVmax values are displayed. **(b)** Average SUVmax values in selected tissues for two animals treated with dual-therapy (ROq14, RIv14)(blue) and two animals treated with ART+ control IgG (RLo14 and RUs14)(copper) at week 23, 5 weeks after ART interruption. **(c)** Average SUVmax values as in **b** for spleen, with representative immuno-PET/CT images of spleen from RIv14 (ART + $\alpha_4\beta_7$ mAb) and RLo14 (ART + control IgG). SUV max values are displayed. Median coefficient of variation (CV) indicated in parenthesis panels b and c.